JOURNAL OF MATERIALS SCIENCE **40** (2005) 847–852

Universal features of grain boundary networks in FCC materials

C. A. SCHUH
Massachusetts Institute of Technology, Department of Materials Science and Engineering, MA, USA 02139

M. KUMAR, W. E. KING
University of California, Lawrence Livermore National Laboratory, Materials Science and Technology Division, CA, USA 94550

Grain boundary character distributions and triple junction distributions have been determined for 70 experimental microstructures, comprising aluminum-, copper-, austenitic iron- and nickel-based alloys in a wide variety of processed states. In these FCC metals, the fraction of coincidence site lattice (CSL) boundaries ranges from about 12% (as for a random Mackenzie distribution) to values as high as 75%. Despite wide variations in composition, processing, and grain size, we find that the grain boundary character distribution and triple junction distributions of these materials have striking similarities, and can be described by just a few parameters. This universality arises due to the highly non-random laws that govern the assembly of the grain boundary network, and due to the kinematic limitation that CSL boundaries arise primarily through twinning.

1. Introduction

Although grain boundary science has historically focused on the structure and properties of individual boundaries, new experimental and computational tools allow for the study of the entire grain boundary network as a dynamic complex system. For example, the advent of automated electron backscatter diffraction (EBSD) has allowed grain boundary misorientations to be assessed on 2-D sections through hundreds or even thousands of grains [1]. New computational methods have allowed a spectrum of grain boundary properties to be included in simulations of, e.g., grain growth [2, 3]. As these techniques improve, there is a general consensus that the full five-dimensional parameter space that describes grain boundary structure must be more thoroughly probed; more accurate description of individual boundaries is expected to lead to better understanding and prediction of the boundary network as a whole. At the same time, we have found that like most complex systems, grain boundary networks have universal features that are dictated by simple constraints, and obey straightforward scaling relationships.

Neglecting all five of the geometric parameters that describe the boundary structure, Euler's law places the first topological constraint on the grain boundary network. On a 2-D section, this law dictates that the average number of boundaries per grain is six; for example, five-sided grains can be introduced only if they are compensated by seven-sided grains [4]. Recognizing the crystallographic nature of grain boundaries induces a second, similar conservation law for misorientations. Specifically, misorientations must be conserved at each triple junction, so that a full circuit around the junction yields a net misorientation of zero. In the framework of the coincidence site lattice (CSL) model, this conservation law yields the so-called the *sigma combination rule*, and stipulates that [5–7]:

$$\Sigma a \cdot \Sigma b = m^2 \cdot \Sigma c \tag{1}$$

where Σa, Σb, and Σc are the Σ-values of the three boundaries that meet at the triple junction, denoting the relative size of the coincidence lattice that spans each boundary (see, e.g., Ref. [8] for details on the CSL model). The scalar quantity m can be any common divisor of Σa and Σb. The consistency condition of Equation 1 can also be extended to consider the deviations of each boundary from an ideal low-Σ CSL misorientation, which also obey a combination rule [9]. In either case, this kind of analysis suggests that if the misorientations of two boundaries at the triple junction are known, then the third misorientation is dictated by the need for crystallographic consistency. The above constraints apply to the topology and misorientation of grain boundaries; although a third conservation law must apply to the grain boundary plane or inclination, experimental data from EBSD usually only allows detailed analysis of the grain boundary network in two dimensions.

Finally, apart from these topological laws that constrain the grain boundary network, there is an additional kinematic constraint on the development of CSL boundaries in polycrystals. Because the CSL classification scheme is based entirely on misorientation, CSL

boundaries must develop in a microstructure by a mechanism that involves relative rotations of crystals. Since grain rotation is negligibly slow for crystals with micron or larger grain sizes, CSL boundaries are most often associated with the generation of twins (bounded by $\Sigma 3$ boundaries), which provides a mechanistic means for crystals to rotate. As we will show later, this kinematic limitation has a profound influence on the grain boundary network in FCC materials.

The conceptually simple constraints described above have a strong influence on the topology and crystallographic connectivity among grain boundaries. Thus, although grain boundaries individually exist in a five-dimensional parameter space, the networks assembled from them exhibit surprisingly common characteristics. In the present work, we explore the statistical properties of grain boundary networks from 70 different experimental microstructures, including many alloy compositions and processing histories. We illustrate that for FCC materials, many features of grain boundary networks are quite similar, despite large differences in the material characteristics. We also review recent progress in describing and explaining these universal features of the grain boundary network, and compare these efforts with our new, more exhaustive data set for FCC metals.

2. Experimental methods

The intent of this research was to identify universal statistical features of grain boundary networks, independent of the composition and processing history of the alloys. Accordingly, we have investigated a variety of experimental FCC materials, including pure copper and nickel, as well as various Cu-, Ni-, and austenitic Fe-based alloys. It is important to note that all of these materials are of low- to medium stacking fault energy, and are susceptible to annealing twinning. Only one material of high stacking fault energy was studied (pure aluminum), for comparison with the twin-forming materials.

Since the goal of this work was to identify traits of the grain boundary network that are independent of processing history, we have studied many FCC metals without regard for their processing condition. In almost every case, the alloys were supplied without any information about the exact composition or processing history, although worked, recrystallized, and annealed microstructures were all examined. A few materials that were 'grain boundary engineered' [10–12] to have a high proportion of low-Σ CSL boundaries were also investigated. In total, 70 different microstructures were examined, and the grain sizes of these materials ranged from 2 to 100 μm.

Automated EBSD was used to obtain orientation maps from large sections of each alloy. Typical scans involved more than 50,000 individual data points, covering at least several hundred grains, or more than about 1000 grain boundaries. Custom programs written in IDL (from Research Systems Inc., Boulder, Colorado) were used to calculate the misorientation of each boundary, and Σ values up to 29 were discerned using the Brandon criterion [13, 14]. Custom algorithms were also used to determine the fraction of CSL boundaries (i.e., boundaries with $\Sigma \leq 29$) in a given microstructure, both by length fraction (f_l) and by number fraction (f_n) of boundaries. The coordination of such boundaries at triple junctions was also assessed.

3. Universal features of the grain boundary character distribution

The spectrum of boundary misorientations, or the *grain boundary character distribution* (GBCD), gives quantitative statistical information about the population of individual boundaries. The GBCD has played a major role in studies of grain boundary-controlled deformation and fracture, where low-angle ($\Sigma 1$) and other low-Σ CSL boundaries have been linked to beneficial properties [15–18]. In FCC materials, especially those of low to medium stacking fault energy, the GBCD is often dominated by $\Sigma 3$ boundaries, which arise due to the occurrence of annealing twinning. This is illustrated in Fig. 1, which shows the distribution of low-Σ boundaries for the low to medium stacking fault energy materials, with CSL fractions in the range $f_n = 0.18$ to 0.72. For all of these microstructures the twin boundary ($\Sigma 3$) is dominant, and the "twin variant" $\Sigma 9$ and $\Sigma 27$ boundaries virtually comprise the remainder of the CSL population. As noted by prior authors [10, 19, 20], the other low-Σ CSL boundaries are virtually irrelevant, only very rarely comprising a significant fraction of the boundary population. The dominance of twin boundaries is due to the generation of annealing twins ($\Sigma 3$), which interact to produce $\Sigma 9$ and $\Sigma 27$ boundaries via boundary reactions [21–23].

Given the dominance of twin variant grain boundaries in the low to medium stacking fault energy FCC materials, it is possible to represent the entire GBCD with just a few parameters. For example, one could reasonably describe the microstructure knowing only the fractions of $\Sigma 3$, 9, and 27 boundaries. In fact, we have found that just two parameters can reasonably describe all of the experimental microstructures we have studied

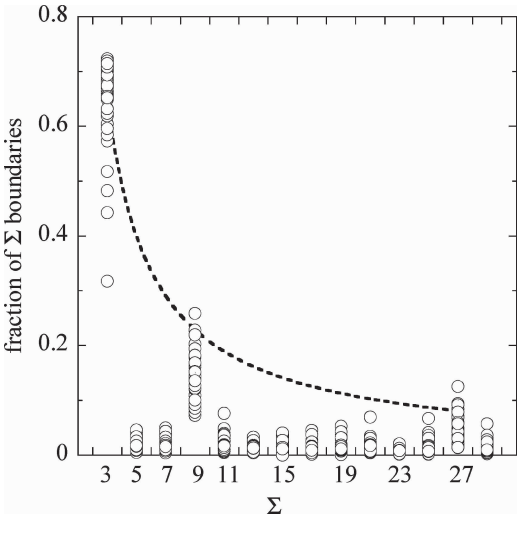

Figure 1 Grain boundary character distribution for 42 low-to-medium stacking fault energy FCC materials, with CSL boundary fractions ranging from $f_n = 0.18$ to 0.72. In each microstructure, twin ($\Sigma 3$) and twin-variant ($\Sigma 9$ and $\Sigma 27$) boundaries are dominant, comprising virtually the entire population of CSL boundaries.

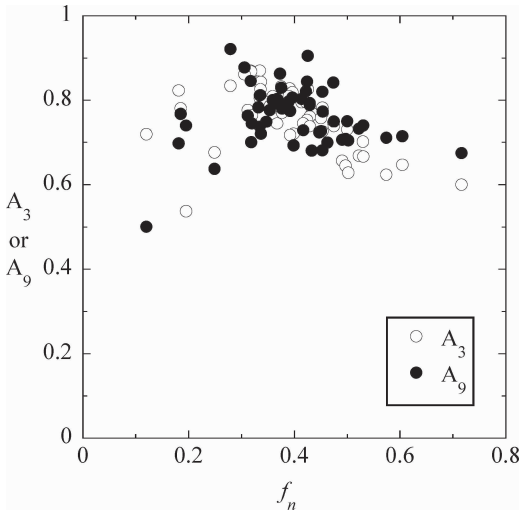

Figure 2 Experimental values of the "twin prominence", A_3, which gives the fraction of $\Sigma 3$ boundaries in relation to the full population of twin-variants. Similarly, A_9 gives the ratio of $\Sigma 9$ boundary fraction to the twin variants, neglecting $\Sigma 3$. The close agreement between these two parameters results from the decay-curve relationship illustrated in Fig. 1, and allows a single value of A to describe the entire population of CSL boundaries in these FCC materials.

to date. This simplification comes by recognizing that the twin-variant boundaries exhibit a geometrically-similar distribution, where $\Sigma 3$ boundaries are most prominent, and the $\Sigma 9$ population is larger than that of $\Sigma 27$ boundaries in roughly the same proportion. Thus, as illustrated schematically in Fig. 1, the data for these boundaries are envisioned to lie on decay-curves that can be described by a single parameter (e.g., a half-life or decay constant). This decaying GBCD is physically justifiable for FCC microstructures that exhibit annealing twinning; two $\Sigma 3$ twin boundaries must interact to produce each $\Sigma 9$ boundary, while a $\Sigma 3$ and a $\Sigma 9$ (i.e., at least three $\Sigma 3$ boundaries) are required to generate a single $\Sigma 27$ boundary. The prominence of $\Sigma 3^{\mathrm{n}}$ boundaries thus decays with the integer value of n. We define a second numerical probability that specifies the *twin prominence*, $A_3 \equiv f_3/(f_3 + f_9 + f_{27})$, where f_{i} denotes the number fraction of boundaries of type Σi.

Fig. 2 plots the experimentally measured value of A_3 for 54 of the experimental microstructures for low to medium stacking fault energy materials. This value is found to be somewhat variable for the different microstructures, but lies in general within a narrow range, $A_3 = 0.5$–0.9. This range brackets the values reported by Gertsman and Tangri [24] for simulated microstructures subjected to multiple twinning events ($A_3 = 0.61$–0.81), as well as a value given by Palumbo *et al.* [25], who considered the efficiency of twinning in producing other low-Σ boundaries and suggested that $A_3 = 2/3$ for the case where each twin boundary coordinates one additional low-Σ boundary. Also shown in Fig. 2 is the ratio $A_9 \equiv f_9/(f_9 + f_{27})$, representing the prominence of $\Sigma 9$ boundaries relative to the $\Sigma 27$ population. If a single parameter could characterize the entire GBCD on the basis of a decaying distribution, then one would expect that $A_3 \approx A_9$. Fig. 2 illustrates that A_9 falls in the same narrow range as A_3, and is usually very close to the numerical value of that parameter. Indeed, for nearly all of the microstructures we have investigated, these two parameters were equal to within 20%. Thus, we find experimentally that a single parameter ($A = A_3 \approx A_9$) can quite reasonably describe the entire distribution of CSL boundaries in low to medium stacking fault energy FCC microstructures.

Coupling the twin prominence, A, with the number fraction of CSL boundaries, f_{n}, the entire GBCD can be reasonably condensed into a simple two-parameter description. In principle, the GBCD should require at least 14 and as many as 21 parameters if different variants of specific CSL boundaries are considered (e.g., $\Sigma 21$a and 21b). The fact that only two parameters can describe the GBCD without a substantial loss of information is somewhat remarkable, and underscores the fact that the network samples some areas preferentially within the vast 3-dimensional space available for grain boundary misorientations. We suggest, therefore, that in the study of individual grain boundaries in FCC metals, the most pertinent investigations will focus on the twin-variant boundaries.

4. The universal relationship between length and number fractions

Previous authors have observed that in FCC materials, the length fraction of CSL boundaries is routinely higher than the number fraction, suggesting that CSL boundaries are longer on average than the population of general high-angle boundaries [10, 26, 27]. This has been of importance from the point of view of ranking microstructures on the basis of their intergranular damage resistance, since the length fraction of boundaries is not expected to correlate simply with, e.g., "secure" triple junction prominence [10, 28]. Kumar *et al.* [10] have pointed out that this inequality is most likely due to the importance of coherent $\Sigma 3$ twin boundaries in such microstructures, which tend to be long and straight, abutting grains composed of shorter boundaries. In the previous section, we showed that the GBCDs for all of the FCC microstructures investigated were surprisingly similar, and the dominance of $\Sigma 3$ boundaries was found to be a universal trait. Consequently, we expect that there should be a simple correlation between the length and number fraction of CSL boundaries, reflective of the universality of the GBCD; this issue is explored further in what follows.

Fig. 3 compares the fraction of CSL boundaries by length and number, as measured from experimental microstructures; in virtually every case the length fraction exceeds the number fraction of CSL boundaries, in agreement with previous research [10]. The only exceptions to this trend occur at low values of f_{n}, approaching the lower limit dictated by the McKenzie distribution ($f_{\mathrm{n}} \sim 0.11$ [29, 30]). In these microstructures, CSL boundaries do not arise through processes involving twinning, but are present in the microstructure by chance. Accordingly, the length and number fractions of these boundaries are quite similar. Another interesting feature of the data in Fig. 3 is that the points are clustered into a single band, and position within that band correlates with the twin prominence,

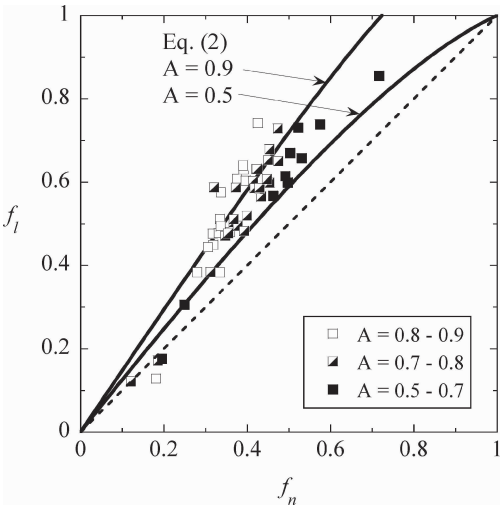

Figure 3 The relationship between the length and number fraction of CSL boundaries for 51 of the experimental microstructures. The high values of f_l occur due to the dominance of long Σ3 boundaries in these microstructures, as captured by the predictions of Equation 2.

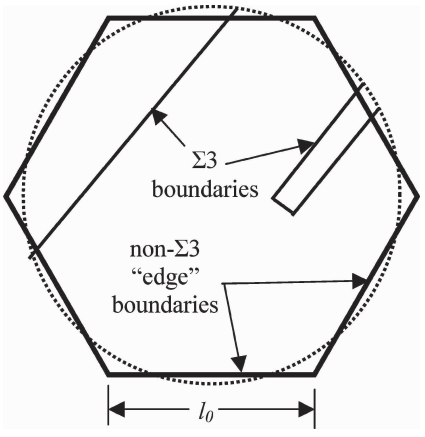

Figure 4 A model 2-D regular hexagonal grain with edge length l_0, containing representative coherent twin boundaries of the grain-spanning and twin-plate variety. Grain-spanning twin boundaries may lie on any chord of the equivalent circular grain (dotted line), which has the same area as the hexagonal grain.

A. At a given number fraction f_n, high values of A are associated with larger length fractions f_l. Since A essentially dictates the density of long Σ3 boundaries, this result is expected.

The universality of the GBCD discussed earlier and illustrated in Fig. 1 translates here into a common trend relating the length and number fraction of special boundaries, where the microstructural variability again exhibits a correlation with the prominence of twin boundaries. As a simple microstructural model to explain this result, we consider a 2-D section in which there are two different average boundary lengths: l_3 is the average length of a Σ3 boundary, and l is the average length of all non-Σ3 boundaries. Then the length fraction of CSL boundaries is given by:

$$f_l = \frac{f_n A l_3 + f_n(1-A)l}{f_n A l_3 + (1-f_n A)l} \tag{2}$$

where A is the 'twin prominence' as described earlier. The above expression can be quantitatively evaluated by introducing a model for how the presence of twin boundaries influences the boundary lengths l_3 and l. Fig. 4 shows an ideal regular hexagonal grain with mean edge length l_0, as well as an equivalent circular grain of the same area, with a radius of $l_0\sqrt{3/\pi}$. Twin boundaries are assumed to have two main morphologies within this ideal grain: twins boundaries can either completely or partially traverse the grain, as shown in the schematic. In either case, the length of twin boundaries will vary depending on their exact position within the grain. Twin boundaries that completely traverse the grain may lie on any chord of the equivalent circular grain, giving an average twin boundary length of:

$$l_3 = 2l_0\sqrt{\frac{3}{\pi}}\int_0^1 \sqrt{1-x^2}dx = l_0\frac{\sqrt{3\pi}}{2} \tag{3}$$

where x is an integration variable describing the perimeter of the circle. We assume that twins which only partially traverse the grain will do so, on average, about half-way across, giving a total twin boundary length very close to that given by Equation 3; the average length of all twin boundaries is therefore reasonably approximated by this expression. This is supported by the numerical ratio of $l_3/l_0 \approx 1.53$ predicted by Equation 3 being in good agreement with the range of experimental values given in Refs. [10, 27] for several Ni-based alloys, stainless steels, and Cr-based alloys ($l_3/l_0 = 1.43$–1.70).

The presence of twins as in Fig. 4 not only creates long Σ3 boundaries, but also divides the hexagon edges into smaller lengths. Therefore, when a microstructure containing N hexagonal edges of average length l_0 is modified by the introduction of T twin boundaries, the total number of boundaries is $N + 3T$. If the resulting microstructure is rescaled so that the average boundary length remains l_0, then we obtain:

$$l = l_0\frac{N + (3 - \frac{\sqrt{3\pi}}{2}T)}{N + 2T} \tag{4}$$

From the definition of A we have:

$$T = N\frac{f_n A}{1 - 3f_n A} \tag{5}$$

Combining Equations 4 and 5 gives the average length of non-Σ3 boundaries as:

$$l = l_0\frac{1 - \frac{\sqrt{3\pi}}{2}f_n A}{1 - f_n A} \tag{6}$$

Equations 3 and 6 respectively describe the inflated length of twin boundaries and the reduced length of non-twin boundaries due to boundary interactions. Using these relationships in Equation 2 then gives a prediction for how the length fraction (f_l) and number fraction (f_n) of CSL boundaries are related. The predictions of Equation 2 are shown in Fig. 3 for the two bounding values of $A = 0.5$ and 0.9. These curves not only exhibit the same general trends with respect to

f_n as the experimental data, but also adequately explain the data variation with changes in the twin prominence, A. Given the great simplicity and many assumptions of this microstructural model, its agreement with experiment reflects the underlying order in complex grain boundary networks.

5. Universal features of the triple junction distribution

Recently, the connectivity among boundaries has been assessed through studies of the triple junction character, by determining the so-called triple junction distribution (TJD) [10, 11, 24, 28, 31]. In this framework, triple junctions are classified by the number of CSL boundaries that coordinate them, giving four different triple junction fractions, J_i, where the integer $i = [0, 3]$ is the number of CSL boundaries. Fig. 5 shows the four triple junction fractions as assessed on 70 different FCC microstructures, plotted as a function of the CSL boundary fraction. Again, we find that despite their breadth of composition and processing history, the specimens all yield triple junction distributions that cluster onto very narrow bands in Fig. 5. Thus, the TJD is another universal feature of the grain boundary network in these materials. Although a similar conclusion has been presented earlier for smaller data sets on just one or two materials [32, 33], the present data represent by far the most exhaustive study of the TJD to date, over the broadest range of f_n and for many different FCC materials.

Also shown in Fig. 5 are solid curves that represent the expected TJD for the case where boundaries are assigned as either CSL or non-CSL boundaries at random. As noted in earlier work [10, 32, 33], these curves are substantially different from the universal trends described by the experimental data, especially in the J_1 and J_2 distributions. Analytical modeling by Minich *et al.* [32] and Monte Carlo simulations by Schuh *et al.* [33] have demonstrated that this non-random nature of the boundary network arises due to the need for crystallographic constraints via Equation 1. For a system of grain boundaries that are predominantly random high-angle and $\Sigma 3^n$ CSL boundaries, there is a strong tendency for the CSL boundaries to cluster because such Σ-combinations as 3, 3, 9 or 3, 9, 27 fulfill the Σ-combination requirement at triple junctions. It is interesting to note that in Fig. 5, the experimental data most closely approach the random distribution at low CSL fractions, below about $f_n \sim 0.3$. It is in these microstructures that twin boundaries become significantly rarer, as the random McKenzie distribution is approached at $f_n \sim 0.11$. Thus, as the GBCD approaches a random distribution, so too does the triple junction distribution.

As a demonstration of the role of crystallographic constraint on the TJD, Fig. 6 reproduces the data from Fig. 5, as well as analytical model predictions based on the model from Ref. [32]. Briefly, the model identifies the triple junction distribution with the maximum informational entropy, using as input the CSL fraction, f_n, and the twin prominence, A. Additionally, this model implements a constraint equivalent to Equation 1, so that the predicted microstructure is guaranteed to be crystallographically consistent. As the results in Fig. 6 demonstrate, the universality of the TJD is readily captured by this model when an average value of $A = 0.70$ (cf. Fig. 2) is used as input. The model curves in Fig. 6 have the same qualitative shape and non-random character as the experimental data points, and are in quite reasonable quantitative agreement as well. When different values of A are used, the model presents a band of solutions that envelop the experimental data [32]. The fact that 70 experimental microstructures all lie on the same curves, and that these data can all be explained by a simple analytical model, suggests a strong underlying order to the complexity of the grain boundary network. In the case of the TJD, this order is imposed by the crystallographic conservation of

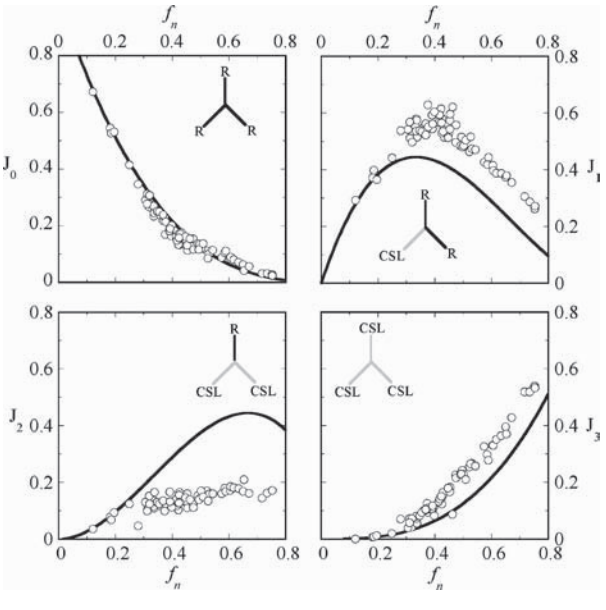

Figure 5 Frequencies of the four triple junction types J_i, where $i = 0$, 1, 2, or 3, denoting the number of CSL boundaries at the junction. Points are derived from all seventy experimental microstructures on FCC materials, and the solid lines are the expected curves based on purely random assembly of the network, without regard to the constraints imposed by crystallography.

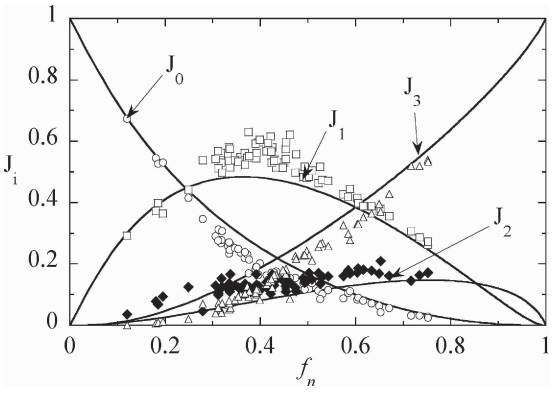

Figure 6 The experimental TJDs from Fig. 5, supplemented by the predictions of the analytical model from Ref. [32] using a single average value of $A = 0.70$. The model captures the strong deviations from linearity associated with a crystallographically constrained network, and even better agreement with the data is possible when a realistic span of A is allowed.

misorientations around each triple junction, as expressed by Equation 1.

6. Conclusions

We have studied the character of grain boundary networks in 70 experimental microstructures, comprising aluminum, copper, nickel, and iron based alloys, in a variety of different microstructural conditions. Despite variations in composition, processing, substructure, grain size, and fraction of CSL boundaries, we have found striking similarities in the grain boundary networks of these microstructures:

1. In low to medium stacking fault energy FCC materials, the CSL grain boundary character distribution (GBCD) is invariably dominated by $\Sigma 3$ boundaries. Because these boundaries arise (and interact) through twinning, they also spawn twin variant $\Sigma 3$ and $\Sigma 9$ boundaries in predictable proportions. In fact, we find that just the CSL fraction and the $\Sigma 3$ fraction are needed to reasonably predict the entire GBCD in these materials.
2. Because the GBCD of these materials is dominated by $\Sigma 3$, the length fraction of CSL boundaries is inflated, as twin boundaries tend to span grains at $\sim$1.5 times the average grain edge length. With a simple geometric model, we predict this effect in reasonable agreement with the experimental data.
3. The triple junctions in FCC materials are non-randomly distributed in terms of their CSL boundary content. However, the triple junction distributions from all of the experimental microstructures fall onto tightly-clustered curves. Although the data are very uniform, they are also highly non-random, an effect stemming from crystallographic constraint and predicted by an analytical model from the literature.

Although there is no question that more meticulous study of individual grain boundaries is needed for detailed prediction of network evolution, we suggest that the above universal aspects of the grain boundary network can potentially narrow the field of focus for future research.

Acknowledgements

Portions of this work were performed under the auspices of the U.S. Department of Energy at the University of California Lawrence Livermore National Laboratory, under contract W-7405-Eng-48 C.S. acknowledges the support of the US National Science Foundation under contract DMR-0346848.

References

1. A. J. SCHWARTZ, M. KUMAR and B. L. ADAMS (Eds.), "Electron Backscatter Diffraction in Materials Science" (Kluwer Academic, New York, 2000).
2. M. C. DEMIREL, A. P. KUPRAT, D. C. GEORGE, G. K. STRAUB and A. D. ROLLETT, *Inter. Sci.* **10** (2002) 137.
3. A. KAZARYAN, Y. WANG, S. A. DREGIA and B. R. PATTON, *Acta Mater.* **50** (2002) 2491.
4. L. J. GIBSON and M. F. ASHBY, "Cellular Solids: Structure & Properties," Second edition (Pergamon Press, Oxford, 1997).
5. K. MIYAZAWA, Y. IWASAKI, K. ITO and Y. ISHIDA, *Acta Cryst.* **A52** (1996) 787.
6. V. Y. GERTSMAN, *ibid.* **A57** (2001) 649.
7. *Idem.*, *ibid.* **A57** (2001) 369.
8. A. P. SUTTON and R. W. BALLUFFI, "Interfaces in Crystalline Materials" (Oxford Science Publication, 1995).
9. M. FRARY and C. A. SCHUH, *Acta Mater.* **51** (2003) 3731.
10. M. KUMAR, W. E. KING and A. J. SCHWARTZ, *ibid.* **48** (2000) 2081.
11. C. A. SCHUH, M. KUMAR and W. E. KING, *ibid.* **51** (2003) 687.
12. *Idem.*, *Zeitschrift für Metallkunde* **94** (2003) 323.
13. D. G. BRANDON, *Acta Metall.* **14** (1966) 1479.
14. M. DESCHAMPS, F. BARIBIER and A. MARROUCHE, *ibid.* **35** (1987) 101.
15. G. PALUMBO and K. T. AUST, in "Materials Interfaces," edited by D. Wolf and S. Yip (Chapman and Hall, London, 1992) p. 190.
16. G. PALUMBO, E. M. LEHOCKEY and P. LIN, *JOM* **50** (1998) 40.
17. T. WATANABE, *Res Mechanica* **11** (1984) 47.
18. *Idem.*, *Mater. Sci. Eng.* **A176** (1994) 39.
19. E. M. LEHOCKEY, G. PALUMBO and P. LIN, *Metall. Mater. Transac.* **29A** (1998) 3069.
20. D. HORTON, C. B. THOMSON and V. RANDLE, *Mater. Sci. Eng.* **A203** (1995) 408.
21. M. KUMAR, A. J. SCHWARTZ and W. E. KING, *Acta Mater.* **50** (2002) 2599.
22. R. L. FULLMAN and J. C. FISHER, *J. Appl. Phys.* **22** (1951) 1350.
23. V. RANDLE, *Acta Mater.* **47** (1999) 4187.
24. V. Y. GERTSMAN and K. TANGRI, *Acta Metallurgica et Materialia* **43** (1995) 2317.
25. G. PALUMBO, K. T. AUST, U. ERB, P. J. KING, A. M. BRENNENSTUHL and P. C. LICHTENBERGER, *Physica Status Solidi* **131** (1992) 425.
26. V. Y. GERTSMAN and K. TANGRI, *J. Mater. Sci. Lett.* **10** (1991) 768.
27. V. Y. GERTSMAN, K. TANGRI and R. Z. VALIEV, *Acta Metallurgica et Materialia* **42** (1994) 1785.
28. P. DAVIES, V. RANDLE, G. WATKINS and H. DAVIES, *J. Mater. Sci.* **37** (2002) 4203.
29. Y. PAN and B. L. ADAMS, *Scripta Metallurgica et Materialia* **30** (1994) 1055.
30. A. MORAWIEC, J. A. SZPUNAR and D. C. HINZ, *Acta Metallurgica et Materialia* **41** (1993) 2825.
31. M. FRARY and C. A. SCHUH, *Appl. Phys. Lett.* **83** (2003) 3755.
32. R. W. MINICH, C. A. SCHUH and M. KUMAR, *Phys. Rev. B* **66** (2002) 052101.
33. C. A. SCHUH, R. W. MINICH and M. KUMAR, *Philosoph. Mag.* **A83** (2003) 711.